Biodistribution and Imaging with ^{123}I-ADAM: A Serotonin Transporter Imaging Agent

Andrew B. Newberg, MD[1]; Karl Plössl, PhD[1]; P. David Mozley, MD[2]; James B. Stubbs, PhD[3]; Nancy Wintering, MSW[1]; Michelle Udeshi, MD[1]; Abass Alavi, MD[1]; Tomi Kauppinen, PhD[4]; and Hank F. Kung, PhD[1]

[1]*University of Pennsylvania, Philadelphia, Pennsylvania;* [2]*Eli Lilly and Company, Indianapolis, Indiana;* [3]*Alpharetta, Georgia; and* [4]*Division of Nuclear Medicine, Helsinki University Central Hospital, Helsinki, Finland*

2-((2-((Dimethylamino)methyl)phenyl)thio)-5-^{123}I-iodophenylamine (^{123}I-ADAM) is a new radiopharmaceutical that selectively binds the central nervous system serotonin transporters. The purpose of this study was to measure its whole-body biokinetics and estimate its radiation dosimetry in healthy human volunteers. The study was conducted within a regulatory framework that required its pharmacologic safety to be assessed simultaneously. **Methods:** The sample included 7 subjects ranging in age from 22 to 54 y old. An average of 12.7 whole-body scans were acquired sequentially on a dual-head camera for up to 50 h after the intravenous administration of 185 MBq (5 mCi) ^{123}I-ADAM. The fraction of the administered dose in 13 regions of interest (ROIs) was quantified from the attenuation-corrected geometric mean counts in conjugate views. Multiexponential functions were iteratively fit to each time–activity curve using a nonlinear, least-squares regression algorithm. These curves were numerically integrated to yield source organ residence times. Gender-specific radiation doses were then estimated with the MIRD technique. SPECT brain scans obtained 3 h after injection were evaluated using an ROI analysis to determine the range of values for the region to cerebellum. **Results:** There were no pharmacologic effects of the radiotracer on any of the subjects, including no change in heart rate, blood pressure, or laboratory results. Early planar images showed differentially increased activity in the lungs. SPECT images demonstrated that the radiopharmaceutical localized in the midbrain in a distribution that is consistent with selective transporter binding. The dose-limiting organ in both men and women was the distal colon, which received an average of 0.12 mGy/MBq (0.43 rad/mCi) (range, 0.098–0.15 mGy/MBq). The effective dose equivalent and effective dose for ^{123}I-ADAM were 0.037 ± 0.003 mSv/MBq and 0.036 ± 0.003 mSv/MBq, respectively. The mean adult male value of effective dose for ^{123}I-ADAM is similar in magnitude to that of ^{111}In-diethylenetriaminepentaacetic acid (0.035 mGy/MBq), half that of ^{111}In-pentetreotide (0.81 mGy/MBq), and approximately twice that of ^{123}I-inosine 5′-monophosphate (0.018 mGy/MBq). The differences in results between this study and a previous publication are most likely due to several factors, the most prominent being this dataset used attenuation correction of the scintigraphic data. Region-to-cerebellum ratios for the brain SPECT scans were 1.95 ± 0.13 for the midbrain, 1.27 ± 0.10 for the medial temporal regions, and 1.11 ± 0.07 for the striatum. **Conclusion:** ^{123}I-ADAM may be a safe and effective radiotracer for imaging serotonin transporters in the brain and the body.

Key Words: ^{123}I-ADAM; radiopharmaceuticals; serotonin transporter; brain; SPECT; dosimetry; radiobiology

J Nucl Med 2004; 45:834–841

In the brain, serotonin participates in the mediation of emotion and cognition. The removal of free serotonin from the synaptic cleft is one of the primary mechanisms for regulating serotonergic tone. Serotonin transporters (5-HTT) are macromolecular complexes that are designed to remove serotonin from the synaptic cleft and move it intact back into the neuronal cytoplasm, where it can be repackaged for reuse or metabolized. Most drugs and diseases induce compensatory changes in transporter function before affecting the concentration of the postsynaptic serotonin receptors. Selective serotonin reuptake receptor inhibitor (SSRI) drugs such as fluoxitine and citalopram have been shown to have significant antidepressant effects (*1*). Hence, the study of this transporter should have significant implications for the study of mood disorders, other psychiatric and neurologic conditions, and the effects of various pharmaceuticals on the serotonergic system.

A few radiopharmaceuticals have been successfully developed for imaging the central nervous system 5-HTT in vivo with 2β-carbomethoxy-3β-(4-^{123}I-iodophenyl)tropane (^{123}I-β-CIT), the most commonly used ligand currently (*2–5*). These radiopharmaceuticals have been labeled with positron-emitting isotopes (*6,7*) or ^{123}I-labeled single-photon emitters as in the case of β-CIT. These agents have been remarkably effective in demonstrating normal (*8–10*) and abnormal neurologic (*11,12*) and psychiatric conditions (*13–15*). Their success has led to efforts to produce more selective (e.g., β-CIT binds to both serotonin and dopamine transporters) and easier-to-use imaging agents for use in conventional medical settings (*16,17*). There has been a considerable interest in the development of selective tracers for imaging 5HTT with PET or SPECT. PET compounds

Received Oct. 15, 2003; revision accepted Dec. 15, 2003.

For correspondence or reprints contact: Andrew B. Newberg, MD, 110 Donner Building, Hospital of the University of Pennsylvania, 3400 Spruce St., Philadelphia, PA 19104.

E-mail: newberg@rad.upenn.edu.

such as ^{11}C-(+)-McN5652 and ^{11}C-3-amino-4-(2-dimethylaminomethylphenylsulfanyl)benzonitrile have been used quantitatively for PET imaging of 5HTT in human brain (*18–21*). In parallel, an equivalent and useful iodinated SPECT imaging agent for 5HTT has not been found, despite several attractive radioiodinated candidates having been reported in the literature (*22–24*). For these reasons, there is a strong impetus to search for a better candidate for imaging 5HTT with SPECT.

2-((2-((Dimethylamino)methyl)phenyl)thio)-5-^{123}I-iodophenylamine (^{123}I-ADAM; Fig. 1) selectively binds the 5-HTT. Biodistribution of ^{125}I-ADAM in rat brain after intravenous injection showed a high specific binding in the regions of hypothalamus, cortex, striatum, and hippocampus, where 5-HTT are concentrated and the specific binding peaked at 120–240 min after injection (*25*). Preclinical studies in nonhuman primates with SPECT have produced midbrain-to-cerebellar ratios of ~2.25:1 (*26*). Overall, the findings have suggested that ^{123}I-ADAM may have several highly advantageous imaging characteristics for visualizing 5-HTT.

Like any other radiopharmaceutical, the use of ^{123}I-ADAM in humans requires estimating its radiation dosimetry—that is, the amount of radiation energy deposited in each organ per unit dose of administered radioactivity (*27*). Image resolution generally improves with higher doses of radioactivity. Enhanced clinical efficacy usually follows as a direct result. Restraint is required, however, because higher doses may incur greater risks of radiation-induced biologic harm. Striking a balance between efficacy and safety requires estimating the radiation doses delivered to each organ in the body. The process of estimating the radiation-absorbed doses requires quantifying the radioactivity distribution within the whole body at multiple time points after administration and developing mathematic models that describe the uptake, retention, and clearance of the radioactivity from each organ of the body (e.g., a biologic model).

An earlier report of the dosimetry of ^{123}I-ADAM in human subjects was published by investigators at the Division of Nuclear Medicine, Helsinki University Central Hospital, in Finland (*28*). However, only 2 subjects were imaged for the full duration of the study, which was only 24 h, with other subjects being imaged at irregular time points and for very short time periods after injection (e.g., <12 h). This has the potential to underestimate the amount of radioactivity remaining in the body at later time points, which could significantly affect the dosimetry. Furthermore, having as many time points as possible should improve the statistical accuracy of the biologic model and, hence, the dose estimates. Also, the earlier report did not factor in attenuation correction, which may significantly affect estimates of the radioactivity in various organs, especially those in areas that are more likely to be affected.

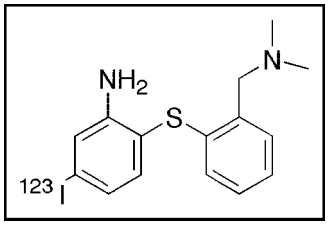

FIGURE 1. Chemical structure of ^{123}I-ADAM.

The purpose of this article is to present a more detailed analysis of the biodistribution, dosimetry, and safety data of the use of ^{123}I-ADAM in human subjects. We also were able to reanalyze the data from the 2 subjects in the Helsinki study to include factors such as attenuation to determine how their values compare with ours. With these data obtained, future studies can be expanded into the clinical setting in the evaluation of patients with a wide variety of neuropsychiatric disorders.

MATERIALS AND METHODS

Accrual and Assessment of Subjects

The design was similar to the design of several others that our laboratory has previously reported (*29–32*). The protocol was approved by the local Committee on Research Involving Humans and the U.S. Food and Drug Administration (Investigational New Drug no. 65,542). Healthy volunteers were recruited through advertisements in local papers and by word of mouth from other volunteers. Medical histories were taken and physical examinations were performed before inclusion. None of the volunteers had a known history of a health problem that could have significantly affected the biodistribution or elimination of the radioligand at the time of study. None of the subjects reported taking any medications at the time of the study other than oral contraceptive pills. All urine drug screens and serum laboratory tests were performed to confirm that individuals were healthy. The final sample included 3 men and 4 women. The average education was 16.4 ± 4.2 y (range, 10–21 y).

Clinical Assessment Procedures

The baseline clinical laboratory tests included a complete blood cell count with differential, serum electrolytes, and liver enzymes. Levels of creatinine, blood urea nitrogen, glucose, cholesterol, triglycerides, albumin, and total protein were also assayed. Pregnancy was ruled out in the women with a urine or serum pregnancy test within 48 h. Routine urinalyses and urine toxicology screens were performed after obtaining explicit consent for drug testing. The blood tests were repeated 4 and 24 h after the administration of the radiopharmaceutical. The urine tests were repeated once after 24 h.

Electrocardiograms (EKGs) were performed 20 min before injection and every 20 min after administration of the radiopharmaceutical up to 1 h. Vital signs (blood pressure, heart rate, pulse oximetry) were taken about every 5 min over the same time interval.

Radiolabeling

No-carrier-added sodium ^{123}I-iodide was obtained commercially (Nordion Inc.). The radionuclidic purity of each dose exceeded 99.8% at the time of delivery. Theoretically, the specific activity of the ^{123}I was 8.7×10^{18} Bq/mol (2.4×10^{8} Ci/mmol).

The radiolabeling process began by adding 100 μL 1.0N hydrochloric acid to a shipping vial containing about 555 MBq (15 mCi) sodium ^{123}I-iodide. The acidified solution was transferred to a kit containing 50 μg of the lyophilized tributyl tin ADAM precursor dissolved in 50 μL ethanol. The iodination was initiated by adding 100 μL 3% hydrogen peroxide solution and quenched 10 min later with 100 μL of a saturated sodium bisulfite solution. The solution was then neutralized with sodium bicarbonate. The reaction mixture was loaded onto a C4 minicolumn (Vydac; Bio-Select Extraction Column, reversed phase), which was activated with 1 mL ethanol and then washed with 3 mL water. The reaction mixture was passed slowly through the C4 minicolumn and the eluent was collected. The column was washed twice with 2 mL water and then washed once with 1 mL 40% ethanol solution. ^{123}I-ADAM was eluted with 0.7 mL ethanol and then diluted with 9.3 mL saline. The final solution was passed through a 0.22-μm sterile filter before administration.

The final product was analyzed for purity by injection of a small amount into a high-performance liquid chromatography column (Hamilton PRP-1 column; 4.1-mm inner diameter × 15-cm length); mobile phase = acetonitrile/3,3-dimethylglutaric acid buffer (5 mmol/L, pH 7), 90:10 ratio; flow rate, 1 mL/min). The retention time for ^{123}I-ADAM was about 14 min and the radiochemical purity was always >90% to be acceptable for administration. Pyrogenicity tests were performed before administration. The unused portion of the final product was retained for sterility tests.

Measurements of Linear Attenuation

An uncollimated transmission source was prepared by dissolving about 1,000 MBq ^{99m}Tc in a 1,600-mL sheet flood made of lucite. ^{99m}Tc was used for its ease and cost knowing that the attenuation coefficient was relatively the same as that for ^{123}I. The rectangular dimensions of the sheet flood were about the same size as the collimators on a dual-head, whole-body camera (Prism 2000; Picker International). The flood was placed flat on top of the posterior projection collimator, and the transmission scan of each subject was performed in the whole-body mode by acquiring images on the upper camera while the sheet source moved with it in tandem on the lower head. The scans were acquired for 10 min each over an excursion length of 214 cm, which corresponded to 25.21 cm/min.

Patient Preparation

Each study began the morning of the first day. Intravenous access was obtained with the subject lying supine on the imaging table. Serum was obtained through the intravenous line after the patient had been lying supine for ~15 min. EKG leads were placed on the subject as well as a blood pressure cuff and pulse oximeter. Subjects were monitored for 20 min before injection of ^{123}I-ADAM and for 60 min after injection.

Emission Images

The radiopharmaceutical was injected rapidly as a bolus through the indwelling intravenous catheter. The first whole-body scan was begun immediately after injection. Each whole-body scan was acquired in a 256 × 1,024 matrix for either 10 or 20 min over a total excursion length of 214 cm. The first 5 scans were acquired for 10 min each. The delayed images were acquired for 20 min. A mean of 12.7 ± 0.5 whole-body images were acquired. Image acquisition was concentrated over the initial 6 h after injection (typically 10 images), and the remaining images were acquired at approximately 24, 30, and 48 h after injection.

SPECT Acquisition

SPECT images of the brain were acquired in subjects ~3½ h after injection for a 1-h scan time on a triple-head camera equipped with fanbeam collimators (Prism 3000XP; Picker International). This time period was selected based on personal communication with the Helsinki researchers, who provided information about the tracer kinetics that suggested the approximate times for image acquisition. The images were reconstructed with a counting rate–dependent restoration filter. The modulation transfer function was generated from the line-spread function of the camera (*33*). Chang's method was used to correct the SPECT scans for attenuation with a uniform ellipse (*34*).

Image Analysis

An operator drew regions of interest (ROIs) around 12 different organs or tissues and the whole body. The regions were drawn on whichever scan showed the organ most clearly. Most organ boundaries were placed on the first whole-body scan. An abdominal ROI was drawn to include the entire abdomen. Thus, the abdominal ROI obtained the maximum activity in the entire gut and it was assumed the activity found its way there via hepatobiliary excretion. Due to blocking with Lugol's solution, the thyroid was not clearly visualized in any of the subjects; therefore, the ROI representing the thyroid was large and stylized to reflect the nonspecific activity in the region of the thyroid fossa. The kidneys were not visualized well in the anterior projection, so the regions for them were placed by flipping the posterior ROIs.

Regardless of which scan the ROI originated from, it was cut and pasted into a single master set. Once the set was complete, the ROIs were transposed onto all other images, including the transmission scans. It was occasionally necessary for an operator to move the entire set of ROIs as a single unit to correct for repositioning errors between scans. It was sometimes necessary to adjust the size of the ROIs for the urinary bladder to account for normal changes in volume with the regions always drawn to include all observable activity (the bladder was always clearly separated from any other areas of activity). The ROI for the body almost always required minor revisions to correct for subject movement, differences in pelvic tilt, and the position of the feet. Otherwise, the individual ROIs were rarely manipulated independently of the other regions in the set. An automated subroutine measured the number of counts in these ROIs. SPECT brain scans were evaluated by applying ROIs on specific brain structures, including the midbrain, medial temporal lobes, and striatum. The counts per area in these regions were compared with cerebellar values.

Calculating Organ Activity

Attenuation corrections were applied from the experimentally measured ratio of counts in the transmission scans of the subjects on the imaging table and the forward decay-corrected counts in the nonattenuated transmission scans through air.

Geometric means for each pair of decay- and attenuation-corrected conjugate ROIs were calculated by multiplying the net anterior counts by the net posterior counts and taking the square root of the product. Decay correction was necessary to compare each time point to the original whole-body activity level. The fraction of the injected dose at each time point was then estimated by dividing the corrected geometric mean number of counts in each ROI by the net geometric mean number of counts in the initial whole-body image.

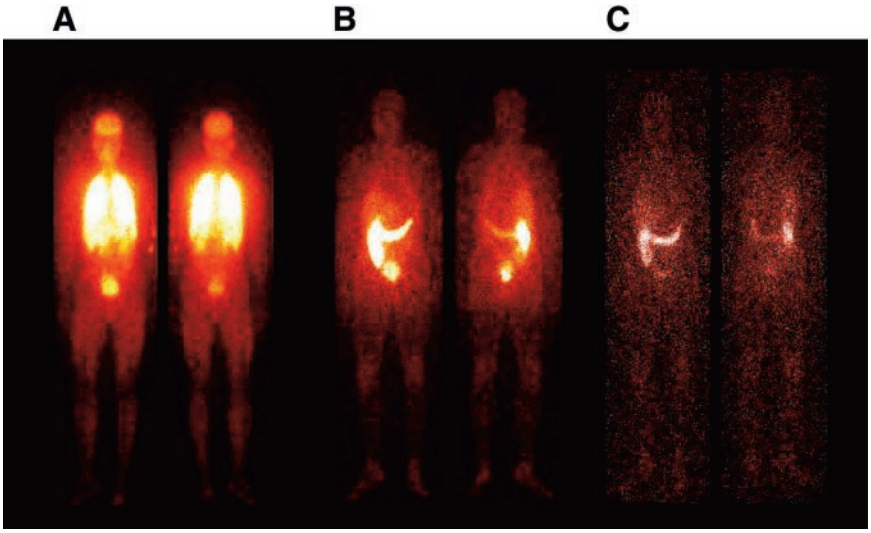

FIGURE 2. Representative anterior (left) and posterior (right) whole-body scans at 20 min (A), 26 h (B), and 48 h (C) after intravenous injection of ^{123}I-ADAM.

Organ Residence Times

Time–activity curves were generated directly from the experimental data for the brain, gallbladder, heart, left kidney, liver, right lung, salivary glands, spleen, thyroid, urinary bladder, and the whole abdominal compartment excluding the urinary bladder (Fig. 2). For this dataset, biexponential functions were iteratively fit to the time–activity curves using a nonlinear least-squares regression algorithm. These were curves numerically integrated to infinity to yield source organ residence times. Whole-body retention was estimated from the ROI encompassing the entire body. Urine was collected from each subject and scintigraphic images were obtained of the collection jugs. However, difficulties in the image acquisition or processing obviated the use of these data, and urinary excretion was subsequently estimated from the total-body clearance. The residence times for the urinary bladder—and thus the dosimetry estimates that followed—were based on a theoretic bladder voiding interval of 4.8 h, or 5 times a day (*35*).

Total fecal excretion was calculated as the maximum percentage of activity in the gut at any image time during the study. The estimated gut radioactivity levels reached their maximum typically by about 24 h. Gallbladder residence times were calculated directly from the time–activity curves, with no accounting for routine voiding of the contents. Thus, gallbladder residence times (and radiation doses) are probably overestimates.

The whole-body time–activity curve was fit to a biexponential function as described; however, the coefficients were constrained to sum to 1.0 (e.g., 100% at time = 0). The total-body clearance parameters are used in computing the urinary bladder residence time. To appropriately account for the fact that a portion of the radioactivity is excreted in the feces rather than in the urine, a correction must be applied to the total-body clearance curve parameters before their use in the dynamic bladder model. The corrected whole (total)-body residence time was calculated by integrating the whole-body time–activity equation, after subtracting the estimated fecal excretion fraction from the coefficient of the slowest clearing total-body component.

The MIRDOSE3.1 software (*36*) was used to estimate the absorbed doses. The urinary bladder was assumed to void regularly at 4.8-h intervals (*37*), a standard assumption for radiopharmaceutical dosimetry analysis (i.e., 5 voidings per day), and the gut transit times of the human adult male and female were assumed (*4*). The MIRDOSE3.1 software has a complete series of dosimetry phantoms corresponding to different age "Reference Human" bodies (*38*). The adult female phantom also serves as the 15-y-old male phantom. All phantoms are hermaphroditic in that each has the full complete of organs, including those of both females and males (e.g., all phantoms have both testes and ovaries and a uterus). The effective dose equivalent (EDE) and effective dose (ED) parameters can be used to compare the radiologic risk associated with low-radiation exposures, such as diagnostic radiology procedures. The organ doses were calculated for each subject individually before the results were averaged.

RESULTS

There were no subjective effects of the radiotracer on any of the volunteers. No changes in vital signs, including heart rate, blood pressure, or pulse oximetry, were observed between the pre- and postinjection measures. There were no changes noted on physical examination. There were no significant changes in EKG findings between pre- and postinjection measures. Specifically, there were no signs of inotropic or chronotropic changes. There were no meaningful changes in any of the clinical laboratory assays that were performed 1, 4, and 24 h after the administration of the tracer. One subject was found to have cocaine in his blood that did not show up initially on laboratory analysis. This subject was evaluated separately but his results were included since the values were entirely consistent with those of the other subjects. Another subject, a 28-y-old woman, had a mild microcytic anemia detected as her hemoglobin count varied slightly around the lower limit of normal, but there were no signs of any effect on hematology.

SPECT brain images showed selective localization in the midbrain and in the medial temporal lobes (Fig. 3), with a lesser degree of uptake in the striatum. A comparison with the corresponding MR images helps to delineate the areas of uptake of ^{123}I-ADAM. Region-to-cerebellum ratios for the brain SPECT scans were 1.95 ± 0.13 for the midbrain,

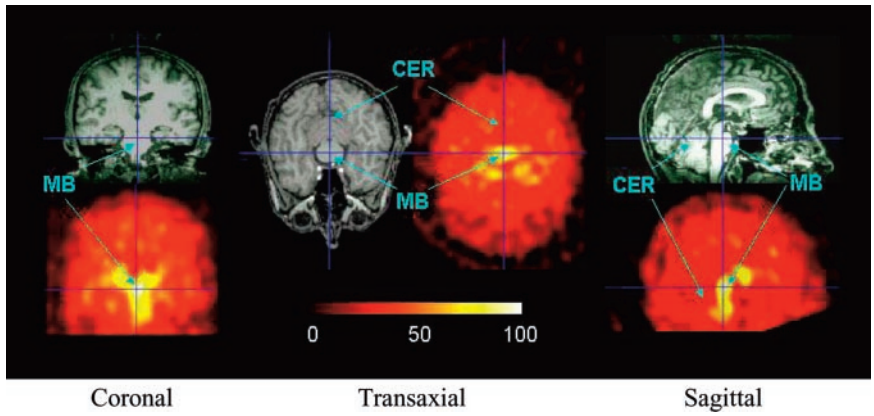

FIGURE 3. SPECT scans of brain acquired 3 h after administration of ^{123}I-ADAM and compared with comparable MR images. MB = midbrain; CER = cerebellum.

1.27 ± 0.10 for the medial temporal regions, and 1.11 ± 0.07 for the striatum.

Planar whole-body images demonstrated increasing activity in the gut that peaked at ~24 h. Radioactivity appearing to be in the gut was clearly transiting through the gut lumen rather than showing a gut wall uptake pattern.

Calculations of the residence times in each organ (Table 1) showed that the largest source organ residence time (other than the total body) was for the liver (mean, 1.21 h; range, 1.08–1.43 h). Tables 2 and 3 list the absorbed-dose estimates for all subjects, using the adult male and the adult female dosimetry phantoms, respectively. The organ receiving the highest estimated dose across all subjects was the distal colon, which, for the adult male phantom, received an estimated 0.098 mGy/MBq (0.43 rad/mCi). Ten organs were estimated to have radiation doses at or above 0.030 mGy/MBq: distal colon, 0.12 mGy/MBq; proximal colon, 0.10 mGy/MBq; bladder wall, 0.067 mGy/MBq; thyroid, 0.055 mGy/MBq; gallbladder wall, 0.052 mGy/MBq; kidneys, 0.050 mGy/MBq; small bowel, 0.044 mGy/MBq; heart and salivary glands, 0.039 mGy/MBq; and liver, 0.031 mGy/MBq. The variability in organ absorbed doses was reasonable, with no organs showing SDs above 20%. Substantially less variability was associated with the mean EDE

TABLE 1
^{123}I-ADAM Residence Times: All Subjects Together

Source organ	Residence time (h)			SD (%)
	Minimum	Maximum	Mean	
Brain	0.238	0.408	0.326	18
Heart	0.099	0.198	0.143	23
Gallbladder	0.337	0.462	0.406	11
Kidneys	0.383	0.589	0.464	18
Liver	1.08	1.43	1.21	9
Lung	0.618	1.052	0.820	22
Spleen	0.091	0.175	0.122	25
Thyroid	0.034	0.066	0.050	20
Salivary glands	0.116	0.176	0.143	15
Urinary bladder	0.534	0.997	0.790	18
Fecal excretion	0.201	0.327	0.243	19
Remainder	2.53	6.53	4.85	32
TB-correct	6.28	10.62	8.53	19
Total body	11.13	14.49	12.37	9

SD = SD expressed as percentage of mean; TB-correct = total-body residence time corrected for fecal excretion fraction.

TABLE 2
^{123}I-ADAM Radiation Doses for Adult Male: All Subjects Together (n = 7)

Source organ	Radiation dose (mGy/MBq)			SD (%)
	Minimum	Maximum	Mean	
Adrenals	9.8E−03	1.4E−02	1.2E−02	13
Brain	8.1E−03	1.2E−02	1.0E−02	15
Breasts	3.8E−03	6.4E−03	5.1E−03	19
Gallbladder wall	4.1E−02	6.5E−02	5.2E−02	16
LLI wall	9.8E−02	1.5E−01	1.2E−01	18
Small intestine	3.9E−02	5.6E−02	4.4E−02	14
Stomach	9.8E−03	1.3E−02	1.1E−02	8
ULI wall	8.6E−02	1.3E−01	1.0E−01	17
Heart wall	3.2E−02	4.5E−02	3.9E−02	11
Kidneys	4.3E−02	6.2E−02	5.0E−02	15
Liver	2.8E−02	3.5E−02	3.1E−02	7
Lungs	2.1E−02	3.2E−02	2.5E−02	18
Muscle	6.6E−03	9.0E−03	7.8E−03	11
Ovaries	2.5E−02	3.2E−02	2.7E−02	10
Pancreas	1.1E−02	1.5E−02	1.2E−02	11
Red marrow	7.5E−03	9.8E−03	8.6E−03	9
Bone surfaces	9.7E−03	1.5E−02	1.3E−02	14
Salivary glands	3.2E−02	4.8E−02	3.9E−02	15
Skin	2.9E−03	5.1E−03	4.1E−03	19
Spleen	2.0E−02	3.3E−02	2.6E−02	18
Testes	5.0E−03	7.3E−03	6.3E−03	14
Thymus	5.3E−03	9.1E−03	7.2E−03	20
Thyroid	3.8E−02	7.3E−02	5.5E−02	20
Urinary bladder wall*	4.9E−02	8.2E−02	6.7E−02	15
Uterus	1.9E−02	2.1E−02	1.9E−02	5
Total body	9.1E−03	1.2E−02	1.0E−02	8
EDE (mSv/MBq)	3.4E−02	4.2E−02	3.7E−02	9
ED (mSv/MBq)	3.3E−02	4.1E−02	3.6E−02	8

*A 4.8-h bladder voiding interval was used in the model.

SD = SD expressed as percentage of mean; LLI = lower large intestine; ULI = upper large intestine.

TABLE 3
^{123}I-ADAM Radiation Doses for Adult Female: All Subjects Together (n = 7)

Source organ	Radiation dose (mGy/MBq)			SD (%)
	Minimum	Maximum	Mean	
Adrenals	1.3E−02	1.8E−02	1.5E−02	12
Brain	8.4E−03	1.3E−02	1.0E−02	15
Breasts	4.6E−03	8.0E−03	6.3E−03	20
Gallbladder wall	4.9E−02	7.6E−02	6.1E−02	16
LLI wall	1.3E−01	2.0E−01	1.5E−01	18
Small intestine	4.9E−02	7.1E−02	5.6E−02	14
Stomach	1.3E−02	1.7E−02	1.5E−02	8
ULI wall	1.1E−01	1.7E−01	1.3E−01	17
Heart wall	4.2E−02	5.8E−02	5.0E−02	11
Kidneys	5.1E−02	7.5E−02	6.0E−02	15
Liver	3.6E−02	4.5E−02	4.0E−02	7
Lungs	3.0E−02	4.6E−02	3.7E−02	18
Muscle	8.3E−03	1.1E−02	9.9E−03	11
Ovaries	3.2E−02	4.2E−02	3.5E−02	11
Pancreas	1.4E−02	1.9E−02	1.6E−02	10
Red marrow	9.1E−03	1.2E−02	1.1E−02	9
Bone surfaces	1.2E−02	1.9E−02	1.6E−02	14
Salivary glands	3.9E−02	5.9E−02	4.8E−02	15
Skin	3.6E−03	6.1E−03	5.0E−03	19
Spleen	2.8E−02	4.6E−02	3.6E−02	18
Testes	6.8E−03	9.6E−03	8.4E−03	12
Thymus	6.6E−03	1.1E−02	8.9E−03	20
Thyroid	6.0E−02	1.2E−01	8.8E−02	20
Urinary bladder wall*	6.3E−02	1.0E−01	8.6E−02	15
Uterus	2.4E−02	2.7E−02	2.5E−02	5
Total body	1.1E−02	1.4E−02	1.3E−02	7
EDE (mSv/MBq)	4.3E−02	5.5E−02	4.8E−02	9
ED (mSv/MBq)	4.4E−02	5.4E−02	4.8E−02	8

*A 4.8-h bladder voiding interval was used in the model.

SD = SD expressed as percentage of mean; LLI = lower large intestine; ULI = upper large intestine.

and ED, which were 0.037 mGy/MBq and 0.036 mGy/MBq, respectively.

DISCUSSION

SPECT scans of the head and planar images of the body suggested that ^{123}I-ADAM selectively binds 5-HTT. ^{123}I-ADAM appears to be pharmacologically safe in healthy volunteers, with no significant physiologic effects noted in laboratory measures, vital signs, or EKGs. This seems appropriate given the relatively small dose of ^{123}I-ADAM actually administered (~21 pmol), which is substantially lower than the milligram doses commonly given for SSRI drugs.

The data obtained for this analysis were acquired using a protocol with biodistribution and dosimetry analyses in mind. This biodistribution study obtained data for ^{123}I-ADAM in 7 subjects. Fecal excretion was taken as the maximum percentage of activity appearing in the abdominal ROI, typically at ~24 h. Urine excretion was estimated from curve fits of the whole-body data.

There were ~13 time points at which radioactivity distributions were obtained scintigraphically. The scheduling of the time points was proper for estimating ^{123}I radiopharmaceutical doses and the schedule was very well followed for all subjects. Imaging was very frequent early (0–6 h after injection), allowing for excellent mathematic modeling of the early, rapid washout phase in the source organs and total body. Images were acquired out to nearly 4 physical half-lives of the ^{123}I, which allows one to accurately model the long-term retention and slow-clearance components. Accurately modeling the slow-clearance components provides substantial improvements in the uncertainties associated with the radiation doses to source organs (slow-clearing components usually account for most of a source organ's residence time). From the biologic models (based on the image data), it appears that little of the ^{123}I is permanently retained in the body or any particular source organs. Even the kidneys, though accumulation continued for often >6 h, eventually begin demonstrating a clearance phase over the final 24- to 48-h time period. The variability of the residence times and radiation doses across all subjects was low (≤20%).

It should be noted that the subjects received thyroid blocking before the administration of ^{123}I-ADAM. Effective thyroid blocking should in theory reduce thyroid uptake of unbound iodide to negligible levels. In addition, during the ROI-drawing process, there were miniscule accumulations of radioactivity visualized in the thyroid and the region referred to as external genitalia in all subjects. As the ROI counts were not background subtracted in the image quantification process, the counts in these 2 regions may simply be soft-tissue background activity. It is also noted that the mean values for thyroid residence time (0.050 h) and all subjects' external genitalia (males, 0.065 h; females, 0.085 h; combined, 0.076 h) are by far the smallest residence times calculated (by a factor of about 2). It should also be noted that the estimates of gallbladder wall dose are overestimates. For the gallbladder contents, it was assumed that no periodic voiding of the gallbladder occurred during the postinjection time period. Clearly, as radioactivity reached the gut lumen, voiding of the gallbladder had occurred.

In internal dosimetry of photon emitters, the contributions to a target organ's radiation dose from activity in the target organ (often called self-dose) is 5–100 times the contribution from photons emitted in nearby source organs (cross-irradiation). This is simply due to the fact that the absorbed fraction for photons emitted in an organ, which are subsequently absorbed by that same organ, is much higher than the absorbed fractions for photons emitted elsewhere and absorbed in the target organ. Specifically assigning even a very small residence time to an organ will thus serve to increase its total radiation dose (summed up over all contributing sources) by a factor of 5–20. For these reasons, we believe it is a reasonable assumption to neglect the external genitalia activity and take the tabulated testes radiation doses (due solely to cross-irradiation from activity in other

source organs) as most probable. Similarly, the thyroid doses are conservative as their residence times were included in the dose calculations. As discussed earlier, the impact on the radiation risk parameters when the testes activity was neglected was to reduce the EDE and ED by ≤10%.

In the 7 subjects studied, estimates of radiation-related risk (EDE and ED) were found to be similar to other nuclear medicine procedures (on a per unit administered activity basis) such as ^{111}In-diethylenetriaminepentaacetic acid (^{111}In-DTPA) (Table 4). The EDE for other iodinated radiopharmaceuticals are also available for comparison: *N*-ω-fluoropropyl-2β-carbomethoxy-3β-(4-iodophenyl)tropane, 0.024 mSv/MBq (*40*); iodobenzamide (IBZM), 0.034 mSv/MBq (*41*); and another group's estimate for ^{123}I-ADAM, 0.021 mSv/MBq (*28*). These values compare with the estimate of EDE, 0.037 mSv/MBq, for the adult male in this study.

The results of the present study showed an estimate for the EDE of ^{123}I-ADAM that is ~50% higher than the previously published value from the Helsinki group. There are several potential reasons for this difference:

- In the current study, attenuation correction was performed. This can be a large factor in adjusting (upward) the estimates of the percentage of injected activity. As one takes the ratio of an organ's geometric mean to that of the total-body geometric mean, some of this factor cancels, though not all.
- In the report from Helsinki (*28*), residence times were calculated using time–activity curves specifically for the small bowel and the distal and proximal colon. We used a larger abdominal ROI to get the maximum activity in the entire gut and assumed it found its way there via hepatobiliary excretion. Furthermore, the gut residence times in our study were computed using a kinetic model, whereas the group from Helsinki did not. For these reasons, our gut doses were somewhat higher than their doses, which may have been another contributing factor in increasing our estimates for ED and EDE.
- The exact same chemical formulations may not have been used in the 2 studies (which could theoretically change the biodistribution, biokinetics, and dose estimates).
- The current study used ~13 times points on each subject, with a concentration during the early times when rapid clearance can be missed, and we acquired images out to 48 h. This may also have contributed to smaller variability and higher estimates for ED and EDE than previously reported.

TABLE 4
Comparison of ED for ^{123}I-ADAM and Other Radiopharmaceuticals

Radiopharmaceutical	ED* (mSv/MBq)
^{131}I-MIBG	0.15
^{67}Ga-Citrate	0.10
^{131}I-Hippuran	0.086
^{111}In-Pentetreotide	0.081
^{123}I-ADAM	0.036
^{111}In-DTPA	0.036
^{99m}Tc-Sulfur colloid†	0.027
^{18}F-FDG	0.024
^{18}F-NaF	0.023
^{99m}Tc-RBCs‡	0.022
^{123}I-IMP	0.018
^{99m}Tc-Disofenin	0.018
^{123}I-MIBG	0.017

*ED is from (*39*) for all radiopharmaceuticals except ^{123}I-ADAM (ED is from this study).

†Oral administration.

‡Heat-treated red blood cells.

MIBG = metaiodobenzylguanidine; IMP = inosine 5′-monophosphate.

In fact, when the Helsinki data were reanalyzed using the mean attenuation correction for the organs obtained in our study as well as the calculated organ residence times using the techniques described in this article, the results were more comparable with our results, with the percentage of injected activity increased in the heart (87%), liver (84%), gallbladder (126%), kidneys (63%), bladder (102%), and gut (41%). The EDE and ED were also more comparable. Thus, attenuation correction appears to have a significant impact on the evaluation of dosimetry.

Evaluation of the brain SPECT scans revealed region-to-cerebellum ratios that were slightly lower than those found during baboon studies (1.95 vs. 2.41, respectively) and were also comparable or even slightly higher than those values reported for other ligands used in human subjects, such as ^{123}I-β-CIT.

CONCLUSION

In general, our findings confirm that it is possible to measure the whole-body biodistribution of ^{123}I-ADAM with greater precision and finer temporal sampling than previously reported. The EDE and ED parameters can be used to compare the radiologic risk associated with low-radiation exposures, and ^{123}I-ADAM compares well with other radiopharmaceuticals. Overall, in addition to the clinical and laboratory data, these results indicate that ^{123}I-ADAM may be a safe imaging agent for studying the 5-HTT in the brain.

ACKNOWLEDGMENTS

This study was partially supported by National Institutes of Health grants AG-17524 and EB-00360. We are also grateful to Aapo Ahonen and his clinical team at the Division of Nuclear Medicine, Helsinki University Central Hospital, Helsinki, Finland, for providing the dosimetry data that formed the basis for our comparison.

REFERENCES

1. Kroenke K, West SL, Swindle R, et al. Similar effectiveness of paroxetine, fluoxetine, and sertraline in primary care: a randomized trial. *JAMA.* 2001;286: 2947–2955.
2. Pirker W, Asenbaum S, Hauk M, et al. Imaging serotonin and dopamine transporters with ^{123}I-β-CIT SPECT: binding kinetics and effects of normal aging. *J Nucl Med.* 2000;41:36–44.
3. Hiltunen J, Akerman KK, Kuikka JT, et al. Iodine-123 labeled nor-beta-CIT as a potential tracer for serotonin transporter imaging in the human brain with single-photon emission tomography. *Eur J Nucl Med.* 1998;25:19–23.
4. Bergstrom KA, Kuikka JT, Ahonen A, Vanninen E. [^{123}I] Beta-CIT, a tracer for dopamine and serotonin re-uptake sites: preparation and preliminary SPECT studies in humans. *J Nucl Biol Med.* 1994;38(4 suppl 1):128–131.
5. Buck A, Gucker PM, Schonbachler RD, et al. Evaluation of serotonergic transporters using PET and [^{11}C](+)McN-5652: assessment of methods. *J Cereb Blood Flow Metab.* 2000;20:253–262.
6. Sandell J, Halldin C, Sovago J, et al. PET examination of [^{11}C]5-methyl-6-nitroquipazine, a radioligand for visualization of the serotonin transporter. *Nucl Med Biol.* 2002;29:651–656.
7. Houle S, Ginovart N, Hussey D, Meyer JH, Wilson AA. Imaging the serotonin transporter with positron emission tomography: initial human studies with [^{11}C]DAPP and [^{11}C]DASB. *Eur J Nucl Med.* 2000;27:1719–1722.
8. Kuikka JT, Tammela L, Bergstrom KA, Karhunen L, Uusitupa M, Tiihonen J. Effects of ageing on serotonin transporters in healthy females. *Eur J Nucl Med.* 2001;28:911–913.
9. Staley JK, Krishnan-Sarin S, Zoghbi S, et al. Sex differences in [^{123}I]beta-CIT SPECT measures of dopamine and serotonin transporter availability in healthy smokers and nonsmokers. *Synapse.* 2001;41:275–284.
10. van Dyck CH, Malison RT, Seibyl JP, et al. Age-related decline in central serotonin transporter availability with [^{123}I]beta-CIT SPECT. *Neurobiol Aging.* 2000;21:497–501.
11. Kim SE, Choi JY, Choe YS, Choi Y, Lee WY. Serotonin transporters in the midbrain of Parkinson's disease patients: a study with ^{123}I-β-CIT SPECT. *J Nucl Med.* 2003;44:870–876.
12. Hesse S, Barthel H, Hermann W, et al. Regional serotonin transporter availability and depression are correlated in Wilson's disease. *J Neural Transm.* 2003;110: 923–933.
13. Tauscher J, Pirker W, Willeit M, et al. [^{123}I] beta-CIT and single photon emission computed tomography reveal reduced brain serotonin transporter availability in bulimia nervosa. *Biol Psychiatry.* 2001;49:326–332.
14. Malison RT, Price LH, Berman R, et al. Reduced brain serotonin transporter availability in major depression as measured by [^{123}I]-2 beta-carbomethoxy-3 beta-(4-iodophenyl)tropane and single photon emission computed tomography. *Biol Psychiatry.* 1998;44:1090–1098.
15. Willeit M, Praschak-Rieder N, Neumeister A, et al. [^{123}I]-Beta-CIT SPECT imaging shows reduced brain serotonin transporter availability in drug-free depressed patients with seasonal affective disorder. *Biol Psychiatry.* 2000;47: 482–489.
16. Oya S, Choi SR, Hou C, et al. 2-((2-((Dimethylamino)methyl)phenyl)thio)-5-iodophenylamine (ADAM): an improved serotonin transporter ligand. *Nucl Med Biol.* 2000;27:249–254.
17. Huang Y, Hwang DR, Narendran R, et al. Comparative evaluation in nonhuman primates of five PET radiotracers for imaging the serotonin transporters: [^{11}C]McN 5652, [^{11}C]ADAM, [^{11}C]DASB, [^{11}C]DAPA, and [^{11}C]AFM. *J Cereb Blood Flow Metab.* 2002;22:1377–1398.
18. Suehiro M, Scheffel U, Dannals RF, Ravert HT, Ricaurte GA, Wagner HN. A PET radiotracer for studying serotonin uptake sites: carbon-11-McN-5652Z. *J Nucl Med.* 1993;34:120–127.
19. Szabo Z, Mohamadiyeh M, Scheffel U, et al. Impulse-response function and kinetic-model of C-11-labeled (+)McN5652 [abstract]. *J Nucl Med.* 1996; 37(suppl):33P.
20. Szabo Z, McCann UD, Wilson AA, et al. Comparison of (+)-^{11}C-McN5652 and ^{11}C-DASB as serotonin transporter radioligands under various experimental conditions. *J Nucl Med.* 2002;43:678–692.
21. Meyer JH, Wilson AA, Ginovart N, et al. Occupancy of serotonin transporters by paroxetine and citalopram during treatment of depression: a [^{11}C]DASB PET imaging study. *Am J Psychiatry.* 2001;158:1843–1849.
22. Jagust WJ, Eberling JL, Biegon A, et al. Iodine-123–5-iodo-6-nitroquipazine: SPECT radiotracer to image the serotonin transporter. *J Nucl Med.* 1996;37: 1207–1214.
23. Kung MP, Chumpradit S, Billings JJ, Kung HF. 4-Iodotomoxetine: a novel ligand for serotonin uptake sites. *Life Sci.* 1992;51:95–106.
24. Mathis CA, Biegon A, Taylor S, Enas J, Hanrahan S, Jagust WJ. [I-125]5-Iodo-6-nitroquipazine: synthesis and evaluation of potent and selective presynpatic serotonin ligand [abstract]. *J Nucl Med.* 1992;33(suppl):890.
25. Choi SR, Hou C, Oya S, et al. Selective in vitro and in vivo binding of [^{125}I]ADAM to serotonin transporters in rat brain. *Synapse.* 2000;38:403–412.
26. Acton PD, Choi SR, Hou C, Plossl K, Kung HF. Quantification of serotonin transporters in nonhuman primates using [^{123}I]ADAM and SPECT. *J Nucl Med.* 2001;42:1556–1562.
27. Sorenson JA, Phelps ME. *Physics in Nuclear Medicine*. 2nd ed. Philadelphia, PA: WB Saunders; 1987:197–218.
28. Kauppinen TA, Bergstrom KA, Heikman P, Hiltunen J, Ahonen AK. Biodistribution and radiation dosimetry of [^{123}I]ADAM in healthy human subjects: preliminary results. *Eur J Nucl Med Mol Imaging.* 2003;30:132–136.
29. Mozley PD, Zhu XW, Kung HF, et al. The dosimetry of 3-iodo-Schering 23390: quantification of the radiation burden to healthy humans. *J Nucl Med.* 1993;34: 208–213.
30. Mozley PD, Stubbs JS, Kung HF, Selickson MH, Stabin MG, Alavia A. Biodistribution and dosimetry of I-123 IBF: a potent radioligand for imaging the D2 dopamine receptor. *J Nucl Med.* 1993;34:1910–1917.
31. Mozley PD, Stubbs JB, Kim H-J, et al. Dosimetry of a D2/D3 dopamine receptor antagonist that can be used with PET or SPECT. *J Nucl Med.* 1995;35:1322–1331.
32. Mozley PD, Stubbs JB, Kim H-J, et al. Dosimetry of an iodine-123-labeled tropane to image dopamine transporters. *J Nucl Med.* 1996;37:151–159.
33. Kim H-J, Karp JS, Kung HF, Mozley PD. Quantitative effects of a count rate dependent Wiener filter on image quality: a basal ganglia phantom study simulating [I-123] dynamic SPECT imaging [abstract]. *J Nucl Med.* 1993;34(suppl): 190P.
34. Chang LT. A method for attenuation correction in radionuclide computed tomography. *IEEE Trans Nucl Sci.* 1978;NS-25:638–643.
35. Cloutier RJ, Smith SA, Watson EE, Snyder WS, Warner GG. Dose to the fetus from radionuclides in the bladder. *Health Phys.* 1973;25:147–161.
36. Stabin M. MIRDOSE: the personal computer software for use in internal dose assessment in nuclear medicine. *J Nucl Med.* 1996;37:538–546.
37. International Commission on Radiological Protection. *Limits for Intakes of Radionuclides by Workers*. ICRP Publication 30: part 1. In: *Annals of the ICRP*. Oxford, U.K.: Pergamon Press; 1979.
38. Cristy M, Eckerman KF. *Specific Absorbed Fractions of Energy at Various Ages from Internal Photon Sources*. ORNL/TM-8381/V1. Oak Ridge, TN: Oak Ridge National Laboratory; 1987.
39. Toohey RE, Stabin MG. Comparative analysis of dosimetry parameters for nuclear medicine. Paper presented at: The 6th International Radiopharmaceutical Dosimetry Symposium; 1996; Gatlinburg, TN.
40. Booij J, Busemann SE, Stabin MG, et al. Human biodistribution and dosimetry of [^{123}IFP-CIT: a potent radioligand for imaging the dopamine transporters. *Eur J Nucl Med.* 1998;25:24–30.
41. Verhoeff NP, Sokole EB, Stabin M, et al. Dosimetry of iodine-123 iobenzamide in healthy volunteers. *Eur J Nucl Med.* 1993;20:747–752.